How Anthropogenic Infrastructure Potentially Alters Terrigenous Sediment Transport Pathways and Fragment River-to-Coast and Alongshore Connectivity - Supplementary Material

Amélie Arias[1*], Rafael Almar[1], Vincent Regard[2], Sebastien Carretier[2], and Edward Anthony[3]

[1]Université de Toulouse, LEGOS (CNES/CNRS/IRD/UT3), Toulouse, France
[2]Université de Toulouse, GET (CNES/CNRS/IRD/UT3), Toulouse, France
[3]CEREGE (Aix Marseille Univ, CNRS, IRD, INRAE, Coll France), Aix-en-Provence, France
[*]Corresponding author: amelie.arias@univ-tlse3.fr

6th July 2025

1. Test case

1.1 Analytical case: Pelnard-Considere groyne

The classical model by Pelnard-Considère (1957) provides a foundational approach to understanding shoreline evolution driven by sediment transported along the coast. It simplifies the process into a one-dimensional diffusion equation by assuming small shoreline deviations, constant wave conditions, and uniform sediment properties:

$$\frac{\partial y}{\partial t} = D\frac{\partial^2 y}{\partial x^2} \quad (1)$$

where y(x,t) is the shoreline position, x is alongshore distance, and D is a diffusion coefficient derived from sediment transport processes

However, while the classical model uses simplified assumptions to derive this equation, it does not explicitly incorporate detailed physical parameters that significantly influence sediment transport, such as wave height, wave period, sediment size, and beach slope. To address these limitations, this study employs the empirical formula of Kamphuis (1991), which explicitly includes these physical parameters, resulting in a more realistic estimation of the diffusion coefficient:

$$Q = AH_b^{2.5}T_p^{0.75}\tan^{0.5}(\beta)d_{50}^{-0.25}\sin(2\theta) \tag{2}$$

In small-angle scenarios, this detailed representation integrates smoothly into the diffusion framework, enhancing the model's physical accuracy. Recognizing the necessity of a robust validation framework that specifically accounts for disruptions such as fully blocking groynes, this study adopts the analytical solution developed byRoelvink & Reniers (2011). Their analytical model precisely captures shoreline evolution in cases of sediment transport interruptions and provides an established benchmark for verifying numerical models. The Roelvink & Reniers (2011) analytical shoreline evolution equation is given by:

$$y^* = [\exp(-x^{*2}) - x^*\sqrt{\pi}(1 - \mathrm{erfc}(x^*))]\,sign(x) \tag{3}$$

$$x^* = \frac{|x|}{\sqrt{4at}}, y^* = \frac{|y|}{\sqrt{4at}}\frac{\sqrt{\pi}}{\varphi'}, a = \frac{S_\infty}{\varphi' d} \tag{4}$$

$$S_\infty = sx\sin(2\varphi') \tag{5}$$

Here, Q_0 denotes the constant sediment transport rate, D_c is the active closure depth, and $erfc$ represents the complementary error function. Using this solution enhances the model's practical relevance and provides a reliable means of assessing its performance against recognized coastal dynamics.

Table 1: Parameters for the groyne test given by Roelvink et al. (2020)

Parameter	**Decription**	**Value**	**Unit**
φ'	wave angle	30	°
d	Profil height	10	m
S_x	Maximum potential of longshore transport rate	500,000	m^3/year/rad
Δx	Grid point spacing	10	m

Figure 1 shows the analytical solution to the test which should be compared with the model result to check the stability and accuracy.

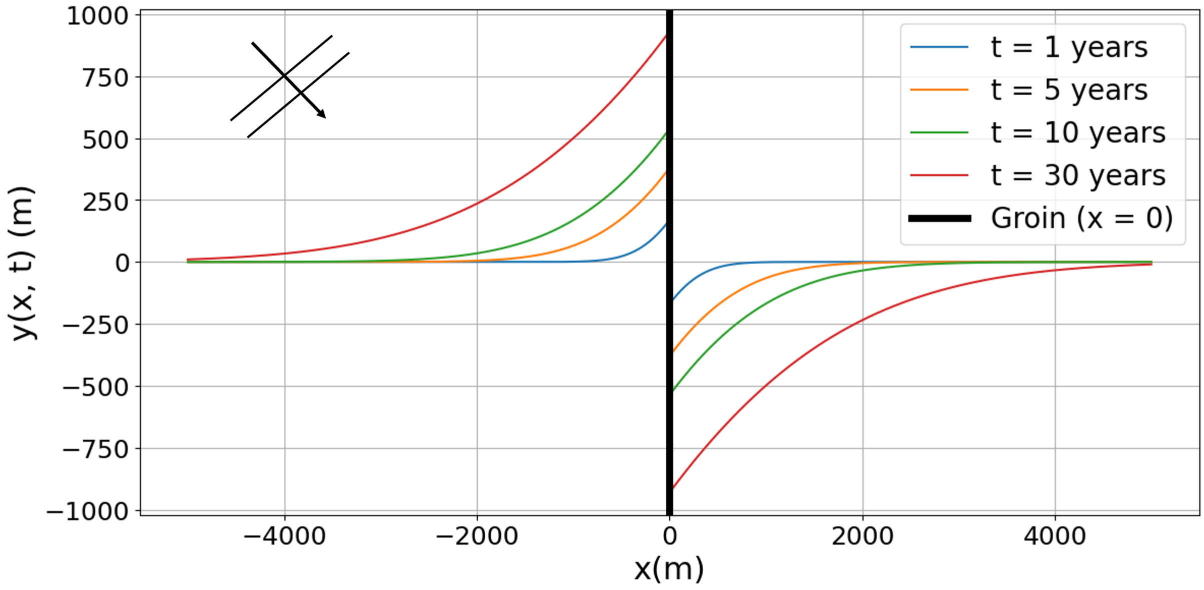

Figure 1: Analytical solution (Eqs. 3-5) of the groyne case with 30° waves.

Figure 2 shows the modeled shoreline evolution over 30 years using the Kamphuis (1991) formulation with a fully blocking groin positioned at the center of the domain. The shoreline clearly exhibits the expected asymmetrical behavior: significant sediment accumulation updrift (to the left of the groin) and erosion downdrift (to the right). The evolution increases smoothly over time, forming the characteristic S-shape often seen in groin-affected shorelines. When compared to the analytical solution of Roelvink & Reniers (2011), the numerical model reproduces the overall spatial pattern and dynamics of shoreline change remarkably well. The position of maximum accretion and erosion aligns spatially, and the smoothing applied yields a physically realistic continuous shoreline. However, there is a slight underestimation of the extent of the downdrift erosion compared to the analytical case, possibly due to spatial smoothing or differences in how transport gradients are distributed near the groin. Overall, the Kamphuis-based numerical model captures the first-order processes and reproduces the analytical shape with good fidelity, validating its use for simulating groin-induced shoreline evolution at decadal scales.

Table 2: Model parameters used in the shoreline evolution simulation

Parameter	**Description**	**Value**	**Unit**
N_{yrs}	Simulation duration	30	years
$zone_{\text{len}}$	Number of alongshore grid points	100	–
dx	Alongshore resolution	100	m
H_s	Significant wave height	1.0	m
T_p	Peak wave period	8.0	s
β	Beach slope	0.05	–
d_{50}	Median grain size	0.0003	m
D_c	Depth of closure	10	m
c	Calibration coefficient	1.0	–
ϕ	Porosity of sediment	0.4	–
ρ_s	Sediment density	2650	kg/m^3
ρ	Water density	1025	kg/m^3

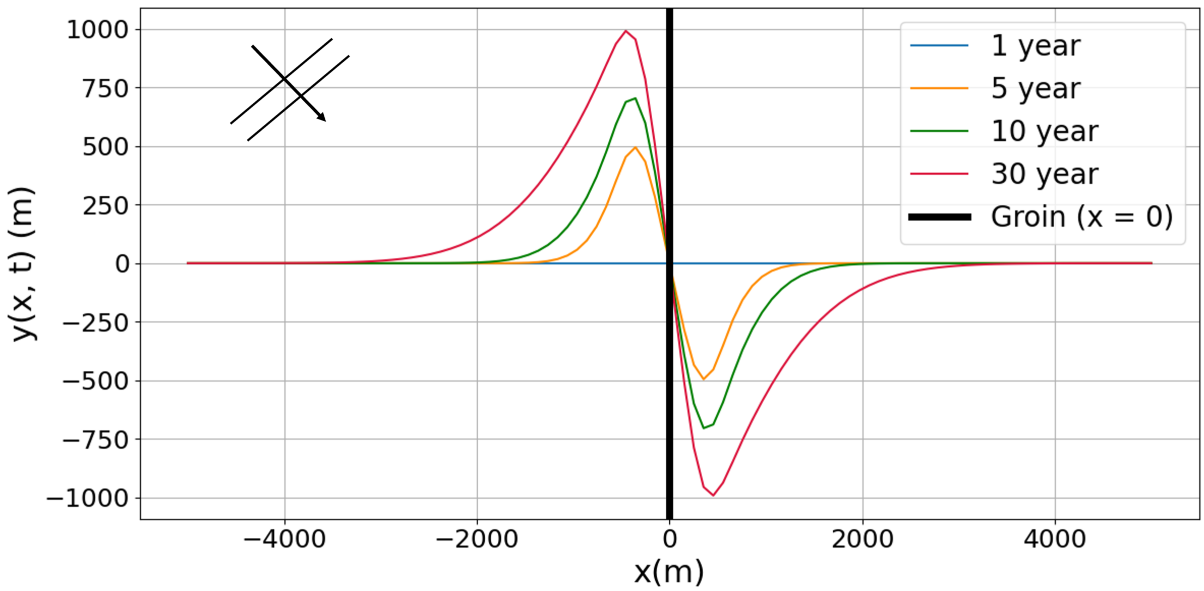

Figure 2: Numerical simulation of shoreline evolution over 30 years using the Kamphuis formulation with a fully blocking groin located at $x = 0$.

Building on this validation, we extend the analysis to more complex and realistic coastal environments using the global implementation of the model. Unlike the idealised 1D shoreline, real-world coastlines have complex morphologies, variable wave climates and a wide range of human interventions. Among these, jetties - often built to stabilise inlets or protect harbour entrances - interact with spatially heterogeneous longshore sediment transport, often leading to significant local and regional changes in sediment budgets. To explore the potential impact of jetties on a global scale, we adopt a deliberately conservative, **high-impact scenario by setting the sediment bypass rate to zero.**This assumption represents a completely blocked structure where no sediment is allowed to pass around or through the jetty. While this configuration may not capture all real-world bypass mechanisms, it allows us to assess the upper bound of sediment disturbance and provides clear insights into how jetties can interrupt natural sediment pathways and reshape sedimentary patterns across entire sediment cells. The following results highlight these dynamics and underline the importance of considering infrastructure-driven sediment redistribution in coastal management and planning.

1.2 Numerical Fluvial Sediment Signal Propagation

In addition to the analytical estimation of lag times, we performed a **numerical experiment** to demonstrate how the model used in this study handles the propagation of a localized sediment signal. Specifically, we introduced a one-time fluvial sediment input ($Q_{continental}$) at a single location and tracked its redistribution over time under the influence of model-derived longshore sediment transport gradients. The experiment was conducted using a simplified one-dimensional transport framework representative of conditions in the Bay of Benin (Figure 3). The injected patch modifies the local sediment transport rate (Q_{lst}) at one point and time step. By running a parallel simulation without the fluvial input, we isolated the signal attributable to the patch alone by computing the difference in transport gradients (ΔQ_{lst}) between the two simulations.

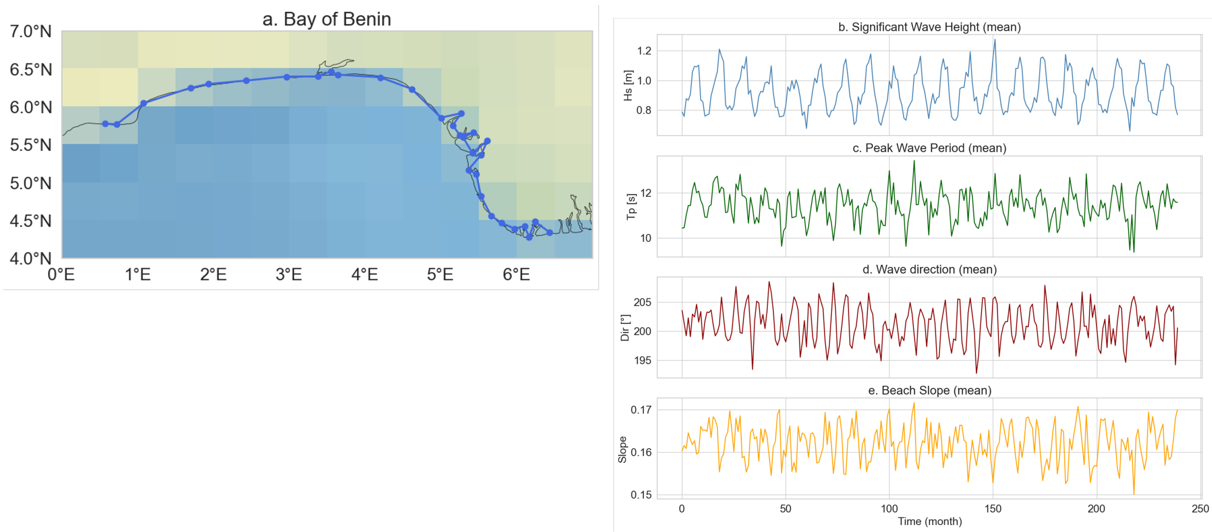

Figure 3: (a) Spatial configuration of the coastline and the locations of offshore sampling points in the Bay of Benin (Gulf of Guinea). The blue dots represent the latitude/longitude points, which are the reference locations used in our dataset. The blue line connecting the dots acts as a proxy for the generalized waterline, closely following the natural coastline and capturing the orientation of the shore. The background color map corresponds to a gridded dataset (e.g., bathymetry or elevation), providing spatial context. This localized map enables precise identification of the segment of the coast analyzed in regional-scale sediment budget and morphodynamic studies.Temporal evolution of key nearshore conditions averaged over the Bay of Benin: (b) Monthly mean of significant wave heights (in meters). (c) Mean peak wave period (Tp- in seconds). (d) Mean wave direction (Dir- in degrees from North).(e) Mean foreshore beach Slope. Time series cover the period January 2000 to December 2019, with values averaged over all shoreline positions within the Bay of Benin region.

Spatio-temporal heatmaps (Figure 4) were generated to visualize the total transport

(Figure 4a)), the transport gradient with and within the sediment river patch (Figure 4b) and Figure (Figure 4c))), and the isolated tracer signal (Figure 4d)).

To assess the capacity of the model to simulate the redistribution of a fluvial sediment input, we injected a sediment patch of $Q_{\mathrm{rivD}} = 10^5\mathrm{m}^3/\mathrm{month}$ at a single coastal location (index 6) in the Bay of Benin and tracked its evolution under the effect of longshore sediment transport (LST). The total transport rate ($KAMP$) in the region ranges between approximately -5.5×10^5 and $+6.5 \times 10^5\mathrm{m}^3/\mathrm{month}$, with strong spatial and temporal variability (Figure 4a). The transport gradient ΔQ_{lst}, noted as $dKAMP$—which governs shoreline change—shows values up to $\pm1\times10^6\mathrm{m}^3/\mathrm{month}$ near the injection point when the patch is present (Figure 4b), while the same area exhibits much lower gradients (maximum $\sim 5\times10^5\mathrm{m}^3/\mathrm{month}$) in the control case without patch injection (Figure 4c). The difference between these two scenarios isolates the impact of the patch (Figure 4d), revealing a strong but highly localized bipolar pattern (one cell seaward, one cell landward), with positive and negative peaks of $\pm10^5\ \mathrm{m}^3/\mathrm{month}$. These values match the injected volume, confirming conservation of mass.

Spatially, the patch remains largely confined to the injection region (±1–2 spatial indices) over the 10-month simulation (4d). The signal exhibits symmetric diffusion, with gradual spreading of the positive/negative dKAMP anomaly. This result confirms that the model can capture the retention and spatial footprint of discrete fluvial sediment events, and that it redistributes them under LST following a physically consistent gradient-driven mechanism. It also demonstrates the limited alongshore reach and persistence of small sediment inputs in weakly forced systems, which may remain localized over multi-month timescales.

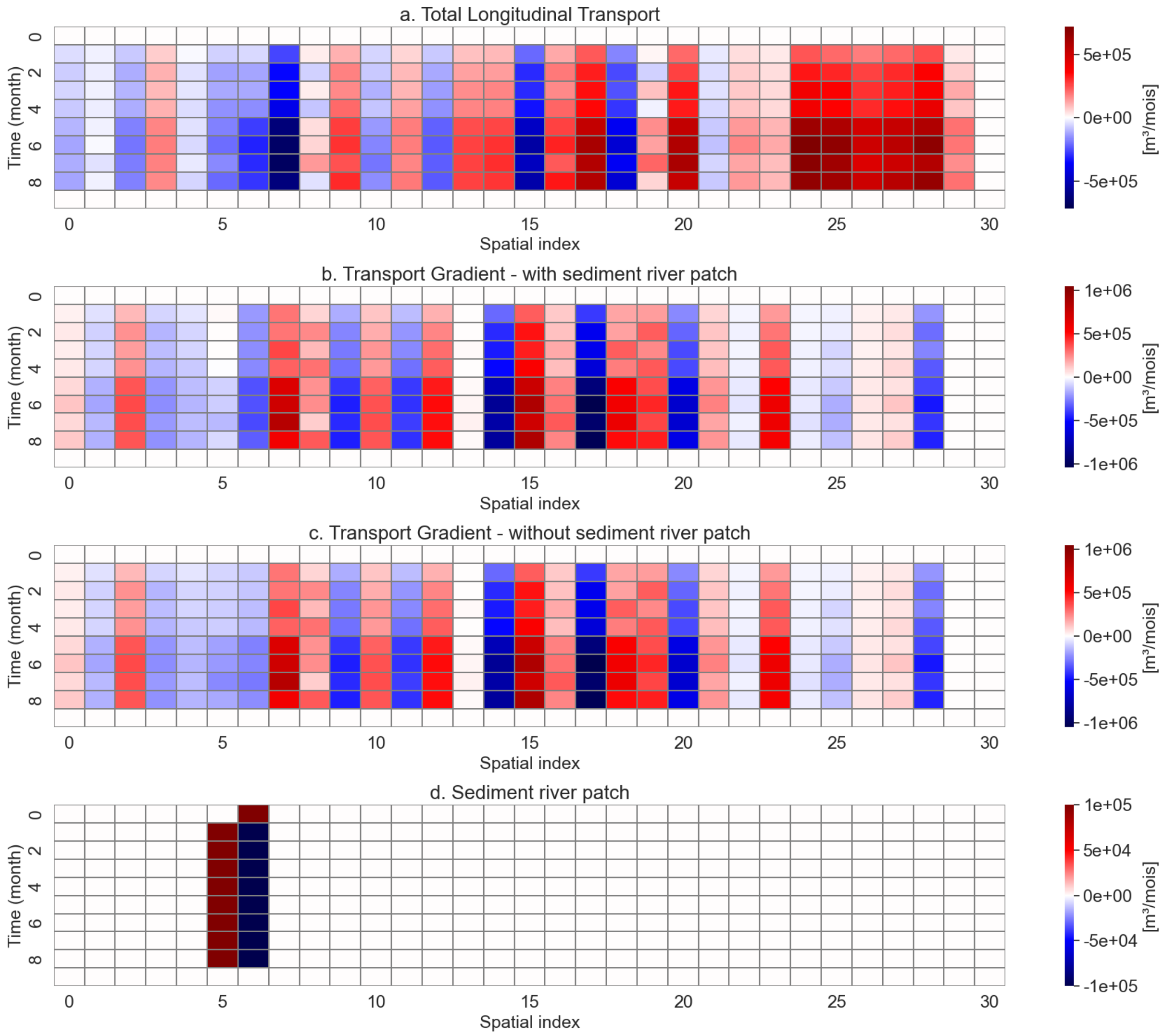

Figure 4: Spatio-temporal evolution of sediment transport in the Bay of Benin in response to a localized fluvial input. A sediment patch of $Q_{\mathrm{rivD}} = 10^5$ m^3/month was injected at coastal index 6 in a simplified 1D transport domain. (a) Longshore sediment transport (Q_{lst}) shows baseline flux magnitudes.(b) Transport gradient ($\partial Q_{lst}/\partial x$) with the sediment input reveals strong localized divergence.(c) Control simulation without the patch highlights natural variability.(d) The difference between (b) and (c) isolates the sediment tracer signal, exhibiting a symmetric bipolar anomaly centered on the injection point. The experiment confirms the model's capacity to conservatively redistribute localized sediment under LST gradients, with limited alongshore dispersion over the 10-month period.

This numerical test confirms that the model is capable of reproducing realistic sediment signal movement through a transport cell. While not intended to validate the lag-time formula per se, the result reinforces the interpretation of lag time as an emergent property of sediment redistribution under longshore transport dynamics. It also illustrates how sediment perturbations may remain spatially confined or take months to years to propagate along the coast—depending on local wave energy, bathymetry, and flux gradients.